# *Hubble Space Telescope* Photometry of Hodge 301: An "Old" Star Cluster in 30 Doradus[1]

Eva K. Grebel [1,2], You-Hua Chu[3]

[1] *University of Washington, Department of Astronomy, Box 351580, Seattle, WA 98195-1580, USA*

[2] *Hubble Fellow*

[3] *University of Illinois at Urbana-Champaign, Department of Astronomy, 1002 West Green Street, Urbana, IL 61801, USA*

## ABSTRACT

We present Hubble Space Telescope Planetary Camera *UVI* data for the little-studied cluster Hodge 301 3′ northwest of 30 Doradus' central ionizing cluster R 136. The average reddening of Hodge 301 is found to be $\langle E_{B-V} \rangle = 0\overset{\mathrm{m}}{.}28 \pm 0\overset{\mathrm{m}}{.}05$ from published infrared and ultraviolet photometry. Using two different sets of evolutionary models, we derive an age of $\sim 20 - 25$ Myr for Hodge 301, which makes it roughly 10 times as old as R 136. Hodge 301 is the most prominent representative of the oldest population in the 30 Dor starburst region; a region that has undergone multiple star formation events. This range of ages is an important consideration for the modelling of starburst regions. Hodge 301 shows a widened upper main sequence largely caused by Be stars. We present a list of Be star candidates. The slope of the initial mass function for intermediate-mass main sequence stars ranging from 10 $M_\odot$ to 1.3 $M_\odot$ is found to be $\Gamma = -1.4 \pm 0.1$ in good agreement with a Salpeter law. There is no indication for a truncation or change of slope of the IMF within this mass range. In accordance with the age of Hodge 301 no obvious pre-main-sequence stars are seen down to $\sim 1\,M_\odot$. We estimate that up to $41 \pm 7$ stars with masses $> 12 M_\odot$ may have turned into supernovae since the formation of the cluster. Multiple supernova explosions are the most likely origin of the extremely violent gas motions and the diffuse X-ray emission observed in the cluster surroundings.

*Subject headings:* Magellanic Clouds – galaxies: star clusters (Hodge 301, R 136) – stars: emission-line, Be – stars: luminosity function, mass function – HII regions

[1]Based on observations made with the NASA/ESA Hubble Space Telescope, obtained at the Space Telescope Science Institute, which is operated by the Association of Universities for Research in Astronomy, Inc. under NASA contract No. NAS5-26555.

## 1. Introduction

Giant HII regions (GHRs) are sites of active star formation and key to understanding starburst phenomena and active galaxies. Their high concentration of massive stars often make them the most prominent regions in distant galaxies. The massive stars are the primary providers of UV ionizing fluxes, kinetic energy, and chemically enriched material. Thorough understanding and correct interpretation of GHRs require the knowledge of their stellar content and star formation history. This can be studied in detail only in nearby GHRs whose stars can be individually resolved.

With a distance of as little as $\sim 50$ kpc 30 Doradus (30 Dor) in the Large Magellanic Cloud (LMC) offers a unique opportunity to study the detailed content of massive stars and star formation processes in a prototypical giant HII region. This starburst region is by far the most luminous and massive star-forming region in the Local Group (Kennicutt 1984) and has been called the Rosetta stone for understanding starburst regions (Walborn 1991). Ground-based and space-based observations have concentrated on 30 Dor's central ionizing cluster, especially its core R 136 (e.g., Parker & Garmany 1993; Malumuth & Heap 1994; Hunter et al. 1995; Brandl et al. 1996; Hunter et al. 1997a; Massey & Hunter 1998; Selman et al. 1999). While these studies yielded significant results for 30 Dor's center, comprehensive understanding of the star formation history in 30 Dor can only be reached by detailed studies of its other clusters and the surrounding field population (e.g., Lortet & Testor 1991; Walborn & Blades 1997; Rubio et al. 1998; Walborn et al. 1999).

Of particular interest for the star formation history of 30 Dor is the previously neglected cluster $\sim 3'$ northwest of R 136 at $\alpha_{2000} = 05^h38^m16^s, \delta_{2000} = -69°03'58''$: Hodge 301 (Hodge 1988; Lortet & Testor 1991; Bica et al. 1999). The most luminous star in this region is the B0.5 Ia supergiant R 132 (Feast et al. 1960), which lies at a projected distance of $\sim 18''$ northwest from the cluster center ($1'' \sim 0.24$ pc). Its cluster membership is uncertain. The three visually brightest stars centered on Hodge 301 were found to be early A supergiants (Melnick 1985). Infrared surveys identified three other luminous stars in Hodge 301 as M supergiants (Mendoza & Gómez 1973; Hyland et al. 1992). Another three stars in Hodge 301 were recently classified as B-type giants and peculiar B main sequence stars (Walborn & Blades 1997). Hodge 301 was not part of the ground-based study of 30 Dor by Parker & Garmany (1993), but was observed with the Ultraviolet Imaging Telescope (*UIT*, Stecher et al. 1992; Hill et al. 1993; Parker et al. 1998). The massive stellar content of Hodge 301 suggests that this cluster belongs to a population older than R 136 (Lortet & Testor 1991; Grebel & Chu 1996; Walborn & Blades 1997). The R 136 cluster began to form low-mass stars 4–5 Myr ago, and its massive stars are as young as 1–2 Myr (Massey & Hunter 1998).

We present here our results for age, stellar content, and initial mass function (IMF) of Hodge 301 based on *Hubble Space Telescope* (*HST*) observations. In Section 2 the data and reduction procedure are described. In Section 3 we derive a mean reddening value for Hodge 301. In Section 4 the age of Hodge 301 is determined using two different sets of evolutionary models. The massive stellar content, in particular the Be stars, are discussed. In Section 5 the mass function of Hodge 301 is derived and its initial massive stellar content is estimated. In Section 6 we briefly discuss the cluster in the framework of the star formation history of 30 Dor, followed by a summary in the final section.

## 2. Observations and Reduction

Hodge 301 was observed on 1995 December 17 with the Planetary Camera (PC) of the Wide Field Planetary Camera 2 (WFPC2; Trauger et al. 1994) aboard *HST* (PI: Chu). The PC chip covers an area of $36\farcs4 \times 36\farcs4$ with a scale of $0\farcs0455$ per pixel. The log of the observations is given in Table 1. Long exposures were split into two frames for efficient cosmic ray rejection.

The aforementioned central coordinates of Hodge 301 are from Bica et al.'s (1999) revised list of LMC clusters. Our own visual estimate of the cluster center based on the Digitized Sky Survey (DSS) yields $\alpha_{2000} = 05^h38^m17^s, \delta_{2000} = -69°04'$ (measured with the IRAF[2]/PROS task TVLABEL), close to the value of Bica et al. (1999). We estimate that the DSS coordinates are accurate to $\sim 2''$ in each coordinate. The central coordinates of our PC chip pointing are

[2]IRAF is distributed by the National Optical Astronomy Observatories, which are operated by the Association of Universities for Research in Astronomy, Inc., under cooperative agreement with the NSF.

$\alpha_{2000} = 05^h38^m17^s, \delta_{2000} = -69°04'03''$. Bica et al. (1999) specify an apparent cluster diameter of $45''$ (major axis = minor axis), while we estimate an approximate diameter of $32'' \pm 5''$ (from the DSS, measured where the intensity level becomes indistinguishable from the background). The useable field of view of the PC is $\sim 34' \times 34'$. Thus our pointing is very close to the apparent cluster center, and the PC chip may be expected to enclose the majority of the cluster stars. Our PC field was positioned such that the brightest star in the region, R 132, is outside our field of view to minimize overexposure effects (Figure 1). Our field contains most of the A and M supergiants and two peculiar B stars (Walborn & Blades 1997).

We used the calibrated images created by the standard *HST* pipeline processing and reduced them with IRAF and STSDAS routines. After cosmic ray removal, the images were corrected with the corresponding position- and intensity-dependent CTE ramps (Holtzman et al. 1995) and with geometric distortion images from the WFPC2 archives.

Stellar photometry was carried out using DAOPHOT2 (e.g., Stetson 1992) running under IRAF. Stars not found by the search routines were added by hand after visual inspection of their profiles. Similarly, cosmics not rejected by the IRAF routines were removed by hand based on their profiles. Point-spread-function (PSF) fitting with a linearly varying Lorentzian PSF was found to leave the smallest residuals. Aperture corrections were determined through aperture photometry with Holtzman et al.'s (1995) aperture sizes and sky annuli on well-isolated, neighbor-subtracted stars on our short exposures.

The transformation relations given in Holtzman et al.'s (1995) Table 7 were used to transform iteratively from the WFPC2 flight system to ground-based *UVI* colors. The F656N images were not transformed.

## 3. The mean extinction of Hodge 301

McGregor & Hyland (1981) list extinctions for the three red supergiants in Hodge 301 (Table 2). For a mean value of $\langle A_V \rangle = 0\overset{\mathrm{m}}{.}96 \pm 0\overset{\mathrm{m}}{.}04$ and a ratio of total to selective extinction $R = 3.5$ (Hyland et al. 1992) their data yield $\langle E_{B-V} \rangle = 0\overset{\mathrm{m}}{.}27 \pm 0\overset{\mathrm{m}}{.}01$. $R = 3.5$ is valid for stars with $(J-K) > 0\overset{\mathrm{m}}{.}75$.

Hill et al. (1993) observed 30 Dor with the *UIT* in the B5 (1615Å), A2 (1892Å), A4 (2205Å), and A5 (2558Å) wavebands. These authors used the UV and ground-based $B$-band photometry to estimate spectral types and reddenings. They adopted a foreground Galactic extinction of $E_{B-V,\mathrm{MW}} = 0\overset{\mathrm{m}}{.}06$ and an LMC halo extinction of $E_{B-V,\mathrm{LMChalo}} = 0\overset{\mathrm{m}}{.}04$ from Heap et al. (1991). LMC-internal extinctions were determined using the reddening curve of Fitzpatrick (1985: F) for 30 Dor and the nebular extinction curve of Fitzpatrick & Savage (1984: FS) together with an ultraviolet spectral library. The total reddening for each of these stars is the sum of the individual extinction values along the line of sight, i.e., $E_{B-V,\mathrm{tot}} = E_{B-V,\mathrm{MW}} + E_{B-V,\mathrm{LMC\,halo}} + E_{B-V,\mathrm{F}} + E_{B-V,\mathrm{FS}}$. Since the full width at half maximum of the stellar images in the *UIT* data ranges from $2\overset{''}{.}5$ to $3\overset{''}{.}0$ not all of the *UIT* objects could be identified unambiguously in our WFPC2 images. Some of the blue stars have the red supergiants as sufficiently close neighbors that light from both contributes to the measured light at *UIT* resolution. We have five stars in the PC chip in common with the *UIT* photometry (stars 247, 256, 257, 259, 264 in Hill et al.'s designation), which are neither close neighbors of M supergiants nor are known to be variable.

Table 2 contains a compilation of cross identifications, spectral classifications, and reddenings for stars in Hodge 301. Column 1 lists the star numbers of Mendoza & Gómez (1973), column 2 identifications by McGregor & Hyland (1981), column 3 by Melnick (1985), column 4 by Hyland et al. (1992), column 5 by Hill et al. (1993), and column 6 by Walborn & Blades (1997). Column 7 gives spectroscopically determined spectral types. In column 8 spectral types derived from Hill et al.'s (1993) *UIT* photometry are listed. Note that the classifications based on *UIT photometry* can deviate significantly from the optical spectroscopy. Extinctions determined by McGregor & Hyland (1981) are given in column 9. The reddenings found by Hill et al. (1993, see above) are listed in columns 10 (F) and 11 (FS). The stars within our field of view are labeled in Figure 2.

The five above named blue supergiants and blue main-sequence stars as well as R 132, which is very close to the border of the PC chip, were used to calculate the mean reddening of Hodge 301 based on *UIT* photometry. We find $\langle E_{B-V,\mathrm{tot}} \rangle = 0\overset{\mathrm{m}}{.}29 \pm 0\overset{\mathrm{m}}{.}04$ as mean reddening from *UIT* plus Heap et al.'s (1991) extinction. This results in a mean extinction of $\langle A_V \rangle = 0\overset{\mathrm{m}}{.}96 \pm 0\overset{\mathrm{m}}{.}13$ for $R_V = 3.35$ (valid for B2 V stars, see Grebel & Roberts 1995). The uncertainties are the standard deviation of the *UIT* values. The *UIT* extinction value is in good agreement with the re-

sults for the red supergiants from infrared photometry but shows larger scatter. Note that the *UIT* measurements often combine the light of several blue main-sequence stars. We adopt $\langle E_{B-V} \rangle = 0\overset{\mathrm{m}}{.}28 \pm 0\overset{\mathrm{m}}{.}05$ as mean reddening value for Hodge 301.

The effect of interstellar extinction on a target star depends on the star's spectral energy distribution within a chosen filter. For a detailed description of the temperature dependence of extinction see Grebel & Roberts (1995), whose relations can be used to perform a color-dependent dereddening. The passbands of the WFPC2 broadband filters deviate from Johnson-Cousins $UBV(RI)_{\mathrm{C}}$ passbands. Thus one should in principle deredden the WFPC2 magnitudes before applying the transformation to observed *UVI* colors. Holtzman et al.'s (1995) Table 12 gives extinction in the primary WFPC2 filters as a function of effective temperature. We carried out the corresponding color-dependent dereddening in the WFPC2 filter system and transformed subsequently to the observed *UVI* system. A comparison of magnitudes resulting from color-dependent dereddening prior to transformation to the ground-based system and after transformation to this system showed only small offsets of the order of $0\overset{\mathrm{m}}{.}02$. In the following sections we will use photometry obtained by dereddening in the WFPC2 flight system and transforming subsequently to the ground-based *UVI* system.

Differential reddening may be present across Hodge 301. Since the effects of differential reddening are difficult to disentangle from effects of stellar rotation (Collins & Smith 1985; Collins et al. 1991) and binarity, no attempt was made to deredden stars individually.

## 4. Massive Stellar Content and Age of Hodge 301

Our *V, (V–I)* color-magnitude diagram (CMD) shows a main sequence extending over $\sim 9$ magnitudes in $V$ (Figure 3, upper panel), blue and red supergiants, and a few red giants belonging to the intermediate-age LMC field population ($V \gtrsim 17$ mag, $(V-I) \gtrsim 0\overset{\mathrm{m}}{.}5$). The *V, (U–V)* CMD (Figure 3, lower panel) does not extend to stars as faint as in the *V, (V–I)* CMD. Representative mean error bars are indicated in the CMDs. Spectroscopic spectral classifications (as opposed to *UIT* classifications) of stars contained within the PC chip comprise the supergiants and two bright peculiar B2 stars (Table 2). The main sequence shows considerable scatter at its massive end in the *V, (V–I)* CMD. As we will show in Section 4.3, this is caused mainly by Be stars, but may in part also be caused by differential reddening, rotation, and/or binarity. The cluster is very well resolved in the PC images, and due to its low stellar density crowding should not have much of an effect on the width of the upper main sequence.

### 4.1. The Age of Hodge 301

We used isochrones from the Geneva group (Schaerer et al. 1993) and from the Padua group (e.g., Bertelli et al. 1994) at the mean metallicity of the young LMC population (Z=0.008) to estimate the age of Hodge 301. Isochrones from the two groups have similar input physics, but differ in the nuclear energy generation rates assumed in particular for the $^{12}\mathrm{C}(\alpha,\gamma)^{16}\mathrm{O}$ reaction, which leads to different extensions of the blue loops (cf. Figure 3).

Since the data were dereddened already (Section 3), the remaining ingredients for the isochrone fits are distance and age. The distance of the Magellanic Clouds remains under debate. We adopt here the 'canonical' value of $(m-M)_0 \sim 18\overset{\mathrm{m}}{.}5$ for the LMC (e.g., Westerlund 1997; van den Bergh 1999), and $18\overset{\mathrm{m}}{.}55$ for 30 Dor (Crotts et al. 1995; Panagia 1999).

The Geneva and Padua models were calculated for single, non-rotating stars and should therefore reproduce the blue main sequence envelope in our CMDs. As can be seen in Figure 3 this is indeed the case for the upper main sequence. Since the location of the apparent main sequence turnoff can be affected by binaries and rotation (e.g., Grebel et al. 1996) and is best determined in conjunction with spectroscopy (Massey et al. 1995a) we rely primarily on the blue and red supergiants to age-date Hodge 301. Stars only spend about one tenth of their main-sequence lifetime as supergiants. Supergiants thus allow one to constrain ages more accurately. Note, however, that neither set of isochrones can reproduce the color loci of the reddest supergiants, a shortcoming that is also noticed in ground-based data.

When comparing coeval Padua and Geneva isochrones with ages of the order of $10^7$ years one finds that the main-sequence turnoff and the supergiant locus lie at brighter $V$ magnitudes for the Padua isochrones, which results in higher age estimates for Padua models. The Geneva isochrones indicate an age of 20 Myr for Hodge 301, while 25 Myr is best compatible with

the Padua isochrones. We conservatively estimate the uncertainty of both age determinations to be ±5 Myr.

A comparison of WFPC2 CMDs of R 136 and Hodge 301 is shown in Figure 4. The R 136 data from Hunter et al. (1995) were retrieved from the Astronomical Data Center. The most luminous stars in R 136 are O3, O4, and hydrogen-burning main-sequence WN stars with masses exceeding $120 M_{\odot}$ and ages of only $\sim 1-2$ Myr (Massey & Hunter 1998). Our CMDs indicate that Hodge 301 is about 10 times older than the massive R 136 cluster, which is in good agreement with expectations from spectral classifications for its massive stars (Table 2 and Walborn & Blades 1997). Hunter et al. (1995) and Brandl et al. (1996) found pre-main-sequence (PMS) stars in R 136 with masses of $4 M_{\odot}$ and less (Figure 4: red stars with $M_{V,0} > 0$ mag), whose ages may range from 1–5 Myr. In contrast, in Hodge 301 the main sequence is well-populated down to $M_{V,0} \sim 4$ to 5 mag. The observed luminosity function of Hodge 301 is shown in Figure 5. In a cluster with an age of 20–25 Myr one would expect to find pre-main-sequence stars at masses below $1 M_{\odot}$. Our data of Hodge 301 do not go deep enough to detect such stars with confidence. The stars at $0\overset{\mathrm{m}}{.}5 < (V-I)_0 < 1\overset{\mathrm{m}}{.}2$ and $-2$ mag $< M_V < 1$ mag are the sparsely populated red giant branch and red clump of the old field population.

### 4.2. Two Potential Blue Stragglers

Two luminous blue stars ($13\overset{\mathrm{m}}{.}8 > V_0 > 13\overset{\mathrm{m}}{.}6$) lie above the apparent main-sequence turnoff but below the locus of the two A supergiants. The bluer one of these two stars, WB2 in Walborn & Blades' (1997) nomenclature (see Figure 2 for its position in the cluster and Table 3 for photometry), lies close to the end points of the blue loops of the Geneva isochrones. Based on its position in the CMD one might consider it a subluminous evolved blue supergiant. Alternatively, it may be a blue straggler candidate or a rapid rotator seen pole-on (Collins et al. 1991; Pols & Marinus 1994; Grebel et al. 1996). This star does not show a pronounced H$\alpha$ excess and is not among our Be star candidates (Section 4.3).

Walborn & Blades (1997) classify the other, redder star as a peculiar variable (WB9: B2 V pec var; cf. Table 2). They suggest that WB9 is a spectroscopic binary with a compact companion whose X-ray emission is responsible for the observed He II 4686Å emission. Based on its photometric H$\alpha$ excess (see Section 4.3) we identify this star as a Be star candidate.

While *ROSAT* High-Resolution Imager (HRI) and Position-Sensitive Proportional Counter (PSPC) data (Wang 1995; Norci & Ögelman 1995) did not reveal X-ray point sources in the Hodge 301 region, WB9 may be a Be X-ray binary, whose X-ray emission is below the detection limit of the existing observations. X-ray binaries with compact companions have X-ray luminosities ranging from $10^{34}$ to $10^{38}$ erg s$^{-1}$. We have used the archival *ROSAT* HRI observation rh400779 (PI: Wang; 105 ks exposure) to determine a $3\sigma$ upper limit for the X-ray luminosity of WB9. We multiplied the HRI count rate by a factor of 3 to approximate the PSPC count rate. We used the visual extinction $A_V$ and the canonical gas-to-dust ratio for the Galaxy and the LMC (Bohlin et al. 1978; Fitzpatrick 1986) to derive the H I column density, and used it to approximate the X-ray absorption column density. Finally, we use the energy-to-count conversion factors given in *ROSAT* Mission Description (1991) to convert from count rate to X-ray flux in the 0.1–2.4 keV band. Both power-law models and thermal plasma emission models for temperatures $kT \sim 1$ keV give similar conversion factors, 1 – $3{\cdot}10^{10}$ counts cm$^2$ erg$^{-1}$. For a distance of 50 kpc to the LMC, the $3\sigma$ upper limit on the X-ray luminosity of WB9 is calculated to be $\leq 10^{35}$ erg s$^{-1}$. This $3\sigma$ upper limit is somewhat high for a 105 ks HRI observation because WB9 is superimposed on the bright diffuse X-ray emission from the interior of shell 3 (Section 5.3, Figure 9). If WB9 is indeed an X-ray binary, it must be at a quiescent stage or has an X-ray luminosity near the lower end of the range of luminosity commonly seen.

### 4.3. Be Stars in Hodge 301

Be stars are non-supergiant (luminosity class V to III) B-type stars with H$\alpha$ emission originating in circumstellar disks. Free-free emission in these ionized disks is responsible for (infra-)red and radio excess observed in Be stars. Be stars can be distinguished photometrically from ordinary B stars through their H$\alpha$ excess (e.g., Grebel et al. 1992; Grebel 1997; Keller et al. 1999). We identified Be star candidates from images obtained in the $F656N$ filter. $F555W$ was used as off-band filter, and $(V-I)$ as temperature indicator to distinguish Be stars from red giants/supergiants that may also appear bright in H$\alpha$.

Fig. 6 shows the resulting two-color diagram. The $(V - H\alpha)$ index is uncalibrated. After adding the magnitude difference that corresponds to the difference in filter width between $F555W$ and $F656N$

(see Grebel et al. 1993), the centroid of blue main-sequence stars without H$\alpha$ emission is at $(V - H\alpha) \sim 0$ mag. We consider all stars with $(V - H\alpha) > 0\overset{\mathrm{m}}{.}4$ to be Be star candidates.

The presence of Be stars, effects of rapid rotation and/or binarity, leads to widened upper main sequences in young clusters (Grebel et al. 1996). The Be star fraction among main sequence B stars appears to increase in low-metallicity environments, a possible indication of increased rotational mixing at low metallicities (Maeder et al. 1999). The reddest and more luminous Be stars (i.e., the earliest spectral types; compare Figures 3 and 6) also tend to have the largest $H\alpha$ excess, as one might expect if both Balmer emission and near-infrared excess originate in the circumstellar disks around the Be stars. While the red excess of the brighter Be stars shows up clearly in the *V, (V–I)* CMD, little red excess is seen in the *U, (U–V)* CMDs.

In order to estimate the Be/(B+Be) number ratio as a function of approximate spectral type we used the photometric magnitude/spectral type calibration for B emission-line stars of Zorec and Briot (1991). Note however that this gives only a crude indication of the distribution of B and Be stars with spectral type (for a discussion see Grebel 1997). Histograms of B stars and Be stars as a function of estimated spectral type are presented in Figure 7. The Be/(B+Be) ratio peaks among B stars with the earliest spectral types, where about half of the stars are Be stars. Both total number of Be stars and Be/(B+Be) number ratio decrease toward later spectral types and fainter magnitudes in accordance with other clusters of similar age (e.g., Grebel 1997; Maeder et al. 1999; Fabregat & Torrejon 1999). Due to decreasing Balmer emission strength toward later spectral types and due to the variability of the Be phenomenon our Be star counts should be considered a lower limit of the "true" number of Be stars. Also, our photometric detection method is biased against the detection of very faint Balmer emission.

One of the Be stars (Be4 = WB6) was spectroscopically classified by Walborn & Blades (1997) as a B2 III giant (Table 2). Be stars are often rapid rotators and can appear as giants even though they may still be main-sequence hydrogen-burning stars (Grebel et al. 1996 and references therein).

Table 3 contains coordinates and photometry for Be stars and other bright stars in Hodge 301. Column 1 gives *UIT* star numbers from Hill et al. (1993). The nomenclature introduced by Walborn & Blades (1997) is listed in column 2. Columns 3 and 4 give the coordinates of the stars. The coordinates were measured using the STSDAS task METRIC, which gives an absolute accuracy of $0\overset{''}{.}5$ rms in each coordinate. The positions of the stars on the PC chip relative to each other have an accuracy to better than $0\overset{''}{.}005$ (Keyes 1997). The coordinates of the stars WB1, WB8, and WB11 were measured on images obtained from the Digitized Sky Survey (DSS) using the IRAF/PROS task TVLABEL (estimated accuracy $\sim 2''$ in each coordinate). Column 5 denotes whether we identified a star as a Be star candidate. For stars outside of our field of view the entry is left blank. Columns 6, 7, 8, and 9 give Hill et al.'s (1993) *UIT* photometry in the B5, A2, A4, and A5 bands (1615Å to 2558 Å, Section 3). Their ground-based $B$-band photometry is listed in column 11. A comprehensive catalog of photometry of the LMC in the *UIT* B1 and B5 bands was published by Parker et al. (1998). Their B1 photometry was not included in the present table. Columns 10, 12, and 13 contain our PC photometry results. The $K$-band photometry by McGregor & Hyland (1981) is given in column 14. Figure 2 can be used to identify the stars listed in Table 3.

## 5. The Mass Function of Hodge 301

The mass function is defined as the number of stars $N$ per logarithmic mass $(M/M_\odot)$ interval per unit area per unit time (Scalo 1986). The slope of the mass function is given by $d(\log N)$ / $d(\log (M/M_\odot))$. In this notation a Salpeter (1955) slope $\Gamma = -1.35$.

### 5.1. The Slope of the Mass Function

Unlike the compact, rich R 136 cluster Hodge 301 is a loose uncrowded cluster that is well-resolved in our *HST* images; furthermore, it does not have many severely saturated stars. This makes determinations of its present-day mass function straightforward. Artificial star experiments indicate that the completeness is $\sim 100 - 93\%$ (Figure 5) throughout the entire mass range considered in Table 4 except for the last mass bin, where the completeness drops to $\sim 75\%$. The absence of obvious PMS stars allows us to include most of the observed stars in the PC chip in the determination of the mass function. We assume that all stars observed in the PC chip are members of Hodge 301 except for the few old red giants. A comparison with the LMC field stars found in the

surrounding WF chips shows that the statistically expected contribution of field stars is of the order of 7 – 8 % (1.5 stars for magnitudes brighter than $V_0 = 16$ mag, 2 stars in the 16 mag $< V_0 <$ 17 mag magnitude bin, 4 stars for 17 mag $< V_0 <$ 18 mag, 8 stars for 18 mag $< V_0 <$ 19 mag, etc.).

We confine our estimation of the mass function to stars considered to be main-sequence (core hydrogen-burning) stars based on their position in our CMDs. We assume that all stars lying along the main sequence are coeval including the stars identified as Be star candidates. Though Be stars may spectroscopically appear as giants, we regard the ones within our field of view as main-sequence stars following Grebel et al. (1996). While spectroscopic classifications exist for the most massive stars in Hodge 301, only one potential main-sequence star has a known spectral type (WB6, see Section 4.3). We will therefore assign mass bins based on photometry alone.

We derive the magnitude bins corresponding to the appropriate mass intervals from a Geneva isochrone with an age of 20 Myr and Z=0.008. This procedure implicitly assumes that each star is a single, non-rotating star, which is certainly an oversimplification. Logarithmic mass intervals with the size of $\Delta \log (M/M_\odot) = 0.1$ were chosen. The upper limit of each logarithmic mass bin, the absolute magnitudes, and star counts based on stars detected in both $F555W$ and $F814W$ are given in Table 4. The uncertainties listed there are the square root of the counts. A weighted least-squares fit results in a mass function slope of $\Gamma = -1.38 \pm 0.07$ (Figure 8, solid line). The determination of the slope is based on 819 stars ranging from $10M_\odot$ to $1.26M_\odot$, covering 6.6 magnitudes in $V$. We note that Massey & Hunter (1998) found $\Gamma = -1.3$ to $-1.4$ for stars $> 15M_\odot$ in R 136 in perfect agreement with a Salpeter slope.

The lowest mass bin considered here (1.26 – 1 $M_\odot$; $3\overset{\mathrm{m}}{.}74 < M_V < 4\overset{\mathrm{m}}{.}85$) was not included in the subsequent calculation of the slope of the mass function due to the increasing incompleteness (see above and Figure 5). Also, toward the low-mass end of this mass bin PMS stars may begin to play a role. The highest mass bin in Figure 8 ($M_\odot > 10$; not included in Table 4) contains stars above the apparent main-sequence turnoff. To avoid uncertainties introduced by supergiant mass loss and incompleteness due to evolutionary effects, this bin was not considered in the slope calculation, either, despite its apparently good agreement with the derived mass function.

### 5.2. Estimation of the Initial Massive Stellar Content and Mass of Hodge 301

Since a mass function slope derived from bona-fide main-sequence stars is essentially an IMF slope, we can extrapolate to higher masses to estimate the initial number of massive stars in Hodge 301. The resulting value serves as a crude indication only since a sparse cluster such as Hodge 301 would have had very few very massive stars to begin with, and we have no way of telling up to which mass the IMF was originally populated. Assuming that Hodge 301 had initially stars as massive as $\sim 120M_\odot$ and a uniformly populated IMF, we find that up to $41 \pm 7$ stars ranging from $\approx 12 - 120M_\odot$ may have turned into supernovae since its formation. The uncertainty of this number was derived from Monte-Carlo simulations to better evaluate the effects of small-number statistics and the stochastic nature of the upper mass cut-off of IMFs (see, e.g., Elmegreen 1997).

The total mass of Hodge 301 can be calculated analytically for a chosen mass range and the above derived IMF slope. Monte-Carlo simulations were used to evaluate stochastic effects on the IMF. Within the well-observed bona-fide main-sequence mass bins from $1.26M_\odot$ to $10M_\odot$ we find a total mass of $(2388 \pm 71)$ $M_\odot$. If we assume that the cluster continues to follow a Salpeter IMF down to $0.4M_\odot$, this adds additional $(2359 \pm 235)$ $M_\odot$. This value is highly speculative since we have not established that (1) the slope derived for intermediate-mass stars is valid also for low-mass stars, and (2) the Salpeter law is indeed valid for low-mass stars in Hodge 301 (cf. Miller & Scalo 1979). The estimated number of low-mass stars from $0.4M_\odot$ to $1.26M_\odot$ is $3647 \pm 362$.

Inclusion of the mass range from $10M_\odot$ to $12M_\odot$, which is the highest observed mass bin in Hodge 301 and consists in part of supergiants, adds another $(135 \pm 21)$ $M_\odot$. This results in an estimated present-day cluster mass of $4882 \pm 247$ $M_\odot$ from $0.4M_\odot$ to $12M_\odot$. The true uncertainty is likely larger than this. Extrapolation from $12M_\odot$ to $120M_\odot$ yields $(1110 \pm 464)$ $M_\odot$ and suggests an initial stellar mass of the cluster of $(\sim 6000 \pm 525)$ $M_\odot$.

The estimate of the cluster mass from low-mass stars alone exceeds recent estimates of the total stellar mass of Galactic open clusters such as the Pleiades (Pinfield et al. 1998: $\sim 735M_\odot$, $\sim 100$ Myr) or Praesepe (Raboud & Mermilliod 1998: 300 – 1330 $M_\odot$, $\sim 80$ Myr). On the other hand, Hodge 301 is a lot less

massive than R 136, where some 65 stars with masses around 120 $M_\odot$ were detected, while the cluster follows a normal, Salpeter-like IMF (Massey & Hunter 1998).

### 5.3. Clues About Past Supernova Events

Spectroscopy of star WB9=Be1 (Walborn & Blades 1997) indicates that it may have a compact companion (Section 4.2). As noted by these authors, the companion may be the stellar remnant of one of the earlier supernova events.

The interstellar medium (ISM) around Hodge 301 gives further clues of a violent past. Hodge 301 is located within shell 3 in 30 Dor (Cox & Deharveng 1983). Shell 3 has a diameter of 120 pc, which is comparable to those of typical superbubbles formed by OB associations or clusters in the LMC. Shell 3 nevertheless has two remarkable features: bright diffuse X-ray emission (Wang & Helfand 1991; Wang 1999, see his Figure 3 particularly) and highly supersonic gas motions (Meaburn 1988). Observations of 30 Dor's kinematics show that shell 3 hosts multiple expanding substructures and that some of the substructures have the most extreme expansion velocities, approaching 300 km $s^{-1}$, in 30 Dor (Chu & Kennicutt 1994, see their Figures 7c and 7d). Both the diffuse X-ray emission and violent motions of shell 3 are characteristic of supernova remnants, and the multiple centers of expansion further indicate multiple supernova explosions. These physical properties thus fully support a dynamic interaction between Hodge 301 and the ambient ISM in 30 Dor. To study the details of this interaction, we have mapped the velocity structure of the WFPC2 field using long-slit echelle spectra; these data will be reported in another paper (Chu et al., in preparation).

## 6. Hodge 301 in the Context of 30 Doradus

Walborn & Blades (1997) identify four different spatial and temporal structures in the starburst region of 30 Dor. The Hodge 301 cluster is the most prominent representative of the oldest component. Other recognizable members of this oldest population include a few massive M and A supergiants found mainly to the east and south of the central ionizing cluster (e.g., Westerlund 1961; Mendoza & Gómez 1973; Hyland et al. 1978; McGregor & Hyland 1981; Parker 1993). In Figure 9 we have marked stars with spectroscopic classifications that trace the different subpopulations in 30 Dor. The distribution of K, M, and A stars is representative of the oldest population are shown in the upper left panel of this figure.

Recent *HST* NICMOS observations of 30 Dor (Walborn et al. 1999) confirmed embedded protostars (Walborn & Blades 1987; Hyland et al. 1992; Rubio et al. 1992), and led to the detection of previously unknown small embedded clusters and Bok globules with forming stars. Together with the younger components listed by Walborn & Blades (1997), this demonstrates that star formation in the nearest extragalactic starburst region has occurred repeatedly over the past 20 – 25 Myr and is still continuing.

Hyland et al. (1992) suggested that the massive stars observed today as red supergiants in the vicinity of the R 136 cluster may have triggered the star formation in its birth cloud making it commence from many directions. The multiple HII shells in the 30 Dor periphery, which show pronounced diffuse X-ray emission (Wang & Helfand 1991; Wang 1999; and upper left panel in our Figure 9) and which are likely the result of repeated supernova explosions seem to give further support to an "outside-in" scenario of star formation. The most recent star formation is occurring in the dense filaments surrounding R 136 (examples are marked in the lower right panel of Figure 9). However, there is no clear evidence of sequentially triggered star formation, and it is conceivable that the repeated star formation events occurred *sua sponte* in a clumpy, increasingly turbulent giant molecular cloud.

## 7. Summary and Concluding Remarks

We have analyzed *HST* WFPC2 data of the sparse cluster Hodge 301 in 30 Dor, which lies 3′ northwest of the massive central ionizing cluster R 136. The published spectral classifications of the supergiants in Hodge 301 indicate already that this cluster is not as young as R 136. Depending on the evolutionary models used our photometry yields an age of $25 \pm 5$ Myr (Padua isochrones) or $20 \pm 5$ Myr (Geneva isochrones), which is $\approx 10$ times as old as the age of R 136 as derived from its massive stars.

Hodge 301 contains Be star candidates, which we identified based on their H$\alpha$ excess. The highest Be star fraction is found among the earliest B spectral types at the main-sequence turnoff region, as is typical for clusters in this age range (Grebel 1997). We provide a finding chart and a table with equatorial co-

ordinates and photometry of the Be star candidates. Two stars above the apparent main-sequence turnoff but below the locus of the A supergiants may be blue stragglers. One of them was identified as a possible binary with a compact companion (Walborn & Blades 1997) and shows H$\alpha$ emission in our data. This star may be a Be X-ray binary. We derive a $3\sigma$ upper limit on the X-ray luminosity of WB9 of $\leq 10^{35}$ erg s$^{-1}$ in the *ROSAT* 0.1–2.4 keV band.

We derive a mass function for the main-sequence stars in Hodge 301 spanning a mass range from 10 to 1.26 $M_\odot$ and find a slope of $\Gamma = -1.38 \pm 0.07$. Thus Hodge 301 has a normal mass function slope in excellent agreement with a Salpeter slope and with the results of Massey et al. (1995a) and Hunter et al. (1997b) for young associations and clusters in the Magellanic Clouds ($\Gamma = -1.3 \pm 0.3$). The slope is slightly steeper than what Hunter et al. (1995; 1996) and Selman et al. (1999) found for the intermediate-mass stars in R 136 (slopes ranging from $\Gamma = -1.0 \pm 0.1$ to $-1.25 \pm 0.05$), and steeper than the mean slope in the Milky Way clusters and associations ($\Gamma = -1.1 \pm 0.1$; Massey et al. 1995b). As discussed by Hunter et al. (1997b) and Sagar & Griffith (1998), deviations of this magnitude may be more indicative of the overall uncertainties in the derivation of a mass function and of the corrections applied than of a significant change of slope. Sirianni et al. (1999) suggest that the IMF of R 136 shows a clear flattening below $3M_\odot$. In Hodge 301 no such flattening is observed down to $\sim 1M_\odot$. We estimate the total present-day mass of Hodge 301 to be $4882 \pm 247$ $M_\odot$ from $0.4M_\odot$ to $12M_\odot$ if a Salpeter function with a single slope is indeed valid over this entire mass range.

Extrapolating Hodge 301's mass function to $120M_\odot$ we find that as many as $41 \pm 7$ massive stars may have evolved into supernovae since the cluster was formed. This is consistent with the highly supersonic gas motions and the diffuse X-ray emission in Hodge 301's surroundings, which indicate multiple supernova explosions.

30 Dor is considered a prototypical starburst region. Its complexity illustrates the importance to consider multiple generations of star and cluster formation when interpreting distant, unresolved starburst regions. Their integrated light may be the result of repeated, distinct star formation episodes that may have spanned a few $10^7$ years rather than just one instantaneous star formation event. Their gas kinematics and velocity dispersion depends on their star formation history and the energy feedback from massive stars. Apart from turbulence, thermal broadening and a gravitational component contribute (e.g., Yang et al. 1996). Depending on the evolutionary stage and star formation history of a giant HII region, the proportionality of these three components can be different. The complex evolutionary history and spatial structure should be taken into account in the modelling of GHRs and starbursts, as Thornley et al. (1999) have attempted for 30 Dor.

We thank Wolfgang Brandner for many useful discussions and our referee, Joel Parker, for helpful comments. Nolan Walborn kindly made available spectral classifications prior to publication. We also wish to acknowledge the use of tabulated data distributed by the Astronomical Data Center at NASA's Goddard Space Flight Center and of *ROSAT* HRI data obtained from the High Energy Astrophysics Science Archive Research Center (HEASARC), provided by NASA's Goddard Space Flight Center. Some of the coordinates were measured on an image obtained from the Digitized Sky Survey. The Digitized Sky Surveys were produced at the Space Telescope Science Institute under U.S. Government grant NAG W-2166. The images are based on photographic data obtained using the UK Schmidt Telescope. The UK Schmidt Telescope was operated by the Royal Observatory Edinburgh, with funding from the UK Science and Engineering Research Council (later the UK Particle Physics and Astronomy Research Council), until 1988 June, and thereafter by the Anglo-Australian Observatory. We also acknowledge extensive use of NASA's Astrophysics Data System Abstract Service.

This research was supported by NASA through the grant STI6122.01-94A. EKG acknowledges support by the German Space Agency (DARA) under grant 05 OR 9103 0 and by NASA through grant HF-01108.01-98A from the Space Telescope Science Institute, which is operated by the Association of Universities for Research in Astronomy, Inc., under NASA contract NAS5-26555.

## REFERENCES

Bertelli, G., Bressan, A., Chiosi, C., Fagotto, F., & Nasi, E. 1994, A&AS, 106, 275

Bica, E.L.D., Schmitt, H.R., Dutra, C.M., Oliveira, & H.L. 1999, AJ, 117, 238

Bohlin, R.C., Savage, B.D., & Drake, J.F. 1978, ApJ, 244, 132

Brandl, B., Sams, B.J., Bertoldi, F., Eckart, A., Genzel, R., Drapatz, S., Hofmann, R., Löwe, M., & Quirrenbach, A. 1996, ApJ, 466, 254

Chu, Y.-H., & Kennicutt, R.C., Jr. 1994, ApJ, 425, 720

Collins, G.W., & Smith, R.C. 1985, MNRAS, 213, 519

Collins, G.W., Truax, R.J., & Cranmer, S.R. 1991, ApJS, 77, 541

Cox, P., & Deharveng, L. 1983, A&A, 117, 265

Crotts, A.P.S., Kunkel, W.E., & Heathcote, S.R. 1995, ApJ, 438, 724

Elmegreen, B.G. 1997, ApJ, 486, 944

Fabregat, J., & Torrejon, J.M. 1999, A&A, submitted (astro-ph/9906240)

Feast, M.W., Thackeray, A.D., & Wesselink, A.J. 1960, MNRAS, 121, 25

Fitzpatrick, E.L. 1985, ApJ, 299, 219 (F)

Fitzpatrick, E.L. 1986, AJ, 92, 1068

Fitzpatrick, E.L., & Savage, B.D. 1984, ApJ, 279, 578 (FS)

Grebel, E.K. 1997, A&A, 317, 448

Grebel, E.K., & Chu, Y.-H. 1996, AGAb, 12, 215

Grebel, E.K., Richtler, T., de Boer, K.S. 1992, A&A, 254, L5

Grebel, E.K., & Roberts, W.J. 1995, A&AS, 109, 293

Grebel, E.K., Roberts, W.J., & Brandner, W. 1996, 311, 470

Grebel, E.K., Roberts, W.J., Will, J.M., & de Boer, K.S. 1993, SSRv, 66, 65

Heap, S.R., Altner, B., Ebbets, D., Hubeny, I., Hutchings, J.B., Kudritzki, R.P., Voels, S.A., Haser, S., Pauldrach, A., Puls, J., & Butler, K. 1991, ApJ, 377, L29

Hill, J.K., Bohlin, R.C., Cheng, K.-P., Fanelli, M.N., Hintzen, P., O'Connell, R.W., Roberts, M.S., Smith, A.M., Smith, E.P., & Stecher, T.P. 1993, ApJ, 413, 604

Hodge, P. 1988, PASP, 100, 1051

Holtzman, J., Burrows, C.J., Casertano, S., Hester, J.J., Trauger, J.T., Watson, A.M., & Worthey, G. 1995, PASP, 107, 1065

Hunter, D.A., Shaya, E.J., Holtzman, J.A., Light, R.M., O'Neil, E.J., & Lynds, R. 1995, ApJ, 448, 179

Hunter, D.A., O'Neil, E.J., Lynds, R., Shaya, E.J., Groth, E.J., & Holtzman, J.A. 1996, ApJ, 459, L27

Hunter, D.A., Light, R.M., Holtzman, J.A., Lynds, R., O'Neil, E.J., & Grillmair, C.J. 1997b, ApJ, 478, 124

Hunter, D.A., Vacca, W.D., Massey, P., Lynds, R., & O'Neil, E.J. 1997a, AJ, 113, 1691

Hyland, A.R., Thomas, J.A., & Robinson, G. 1978, AJ, 83, 20

Hyland, A.R., Straw, S., Jones, T.J., & Gatley, I. 1992, MNRAS, 257, 391

Miller, G.E., & Scalo, J.M. 1979, ApJS, 41, 513

Keller, S.C., Wood, P.R., & Bessell, M.S. 1999, A&AS, 134, 489

Kennicutt, R.C. 1984, ApJ, 287, 116

Keyes, T. 1997, HST Data Handbook Vers. 3, Space Telescope Science Institute, Baltimore

Lortet, M.-C., & Testor, G. 1991, A&AS, 89, 185

Maeder, A., Grebel, E.K., & Mermilliod, J.-C. 1999, A&A, 346, 459

Malumuth, E.M., & Heap, S.R. 1994, AJ, 107, 1054

Massey, P., Johnson, K.E., & DeGoia-Eastwood, K. 1995b, ApJ, 454, 151

Massey, P., Lang, C.C., DeGoia-Eastwood, K., & Garmany, C.D. 1995a, ApJ, 438, 188

Massey, P., & Hunter, D.A. 1998, ApJ, 493, 180

McGregor, P.J., & Hyland, A.R. 1981, ApJ, 250, 116

Meaburn, J. 1988, MNRAS, 235, 375

Melnick, J. 1985, A&A, 153, 235

Mendoza, E.E., & Gómez, T. 1973, PASP, 85, 439

Norci, L., & Ögelman, H. 1995, A&A, 302, 879

Panagia, N. 1999, in 'New Views of the Magellanic Clouds", IAU Symp. 190, eds. Y.-H. Chu et al., ASP Conf. Ser., in press

Parker, J.W. 1993, AJ, 106, 560

Parker, J.W., & Garmany, C.D. 1993, AJ, 106, 1471

Parker, J.W., Clayton, G.C., Winge, C., & Conti, P.S. 1993, ApJ, 409, 770

Parker, J.W., Hill, J.K., Cornett, R.H., Hollis, J., Zamkoff, E., Bohlin, R.C., O'Connell, R.W., Neff, S.G., Roberts, M.S., Smith, A.M., & Stecher, T.P. 1998, AJ, 116, 180

Pinfield, D.J., Jameson, R.F., & Hodgkin, S.T. 1998, MNRAS, 299, 955

Pols, O.R., & Marinus, M. 1994, A&A, 288, 475

Raboud, D., & Mermilliod, J.-C., 1998, A&A, 333, 897

*ROSAT* Mission Description 1991, NASA Publication NRA 91-OSSA-25, Appendix F

Rubio, M., Barbá, R.H., Walborn, N.R., Probst, R.G., García, J., & Roth, M.R. 1998, AJ, 116, 1708

Rubio, M., Roth, M., & García, J. 1992, A&A 261, L29

Sagar, R., & Griffiths, W.K. 1998, MNRAS, 299, 777

Salpeter, E.E. 1955, ApJ, 121, 161

Scalo, J.M. 1986, Fundam. Cosmic Phys., 11, 1

Schaerer, D., Meynet, G., Maeder, A., & Schaller, G. 1993, A&AS, 98, 523

Selman, F., Melnick, J., Bosch, G., & Terlevich, R. 1999, A&A, 347, 532

Sirianni, M., Leitherer, C., Nota, A., Clampin, M., & de Marchi, G. 1999, in IAU Symp. 190, "New views of the Magellanic Clouds", eds. Y.-H. Chu et al., ASP Conf. Ser., in press

Stecher, T. P., et al. 1992, ApJ, 395, L1

Stetson, P.B. 1992, in 'Astronomical Data Analysis Software and Systems I', ASP Conf. Ser. 25, eds. D.M. Worrall, C. Biemesderfer, & J. Barnes, p. 297

Trauger, J.T., et al. 1994, ApJ, 435, L3

Thornley, M.D., Lutz, D., Kunze, D., & Spoon, H. 1999, in IAU Symp. 190, "New views of the Magellanic Clouds", eds. Y.-H. Chu et al., ASP Conf. Ser., in press

van den Bergh, S. 1999, in IAU Symp. 190, "New views of the Magellanic Clouds", eds. Y.-H. Chu et al., ASP Conf. Ser., in press

Walborn, N.R. 1991, in IAU Symp. 148 'The Magellanic Clouds', eds. R. Haynes & D. Milne, Kluwer, Dordrecht, p. 145

Walborn, N.R., & Blades, J.C. 1987, ApJ, 323, L65

Walborn, N.R., & Blades, J.C. 1997, ApJS, 112, 457

Walborn, N.R., Barbá, R.H., Brandner, W., Rubio, M., Grebel, E.K., & Probst, R.G. 1999, AJ, 117, 225

Wang, Q.D. 1995, ApJ, 453, 783

Wang, Q.D. 1999, ApJ, 510, L139

Wang, Q.D., Helfand, D.J. 1991, ApJ, 370, 541

Westerlund, B.E. 1961, Uppsala Astron. Obs. Annals, 5, # 1

Westerlund, B.E. 1997, "The Magellanic Clouds", Cambridge University Press, p. 20

Yang, H., Chu, Y.-H., Skillman, E.D., & Terlevich, R. 1996, 112, 146

Zorec, J., & Briot, D. 1991, A&A, 245, 150

This 2-column preprint was prepared with the AAS LaTeX macros v4.0.

Fig. 1.— Location of the WFPC2 field in 30 Doradus. Hodge 301 is contained in the field of view of the PC chip. The long sides of the WFPC2 footprint are $\sim 80''$ long. The underlying image is a composite of a broadband $R$ and an [SII] image obtained with the NTT and EMMI in 1995. The location of the B0.5 Ia star R 132, which lies just outside of the PC chip, is indicated as well.

Fig. 2.— Left: A composite image (*F336W, F555W, F814W*) of Hodge 301 (PC chip). Right: The same image with star identifications. Be star candidates identified through their H$\alpha$ excess are marked by circles. Star numbers from Walborn & Blades (1997) are prefixed by WB and are marked by diamonds unless they were identified as Be stars. The stars from the *UIT* study of Hill et al. (1993) that do not have other identifiers are marked by squares. See text and Tables 2 and 3 for more information. The three concentric circles indicate apertures of $1''$, $2.5''$, and $3''$ to illustrate the crowding problems in the *UIT* data (Section 3).

Fig. 3.— $(V-I)_0$, $V$ (upper panel) and $(U-V)_0$, $V$ (lower panel) color-magnitude diagrams (CMDs) of Hodge 301 with Geneva (left) and Padua isochrones (right) at Z=0.008. B emission-line stars are indicated through grey dots (Section 4.3). Stars brighter than $V = 14$ mag were plotted as fat dots to retain legibility. Representative error bars are plotted in the left-hand side of each CMD. An age of 20–25 Myr (solid lines) seems best compatible with the isochrones.

Fig. 4.— Comparison between the color-magnitude diagrams of R 136 (data taken from Hunter et al. 1995 and dereddened using their values) and Hodge 301. Both datasets were obtained with WFPC2 and have the same exposure times. Geneva group isochrones for Z=0.008 are overplotted as solid lines. A pre-main-sequence (PMS) track is shown for R 136 as a dashed line. PMS stars can be seen in the R 136 diagram at $M_{V,0} \sim 0\overset{\mathrm{m}}{.}3$ and fainter magnitudes. At $M_{V,0} \gtrsim 3\overset{\mathrm{m}}{.}5$ the contribution from PMS stars becomes dominant. No such trend is seen in the much older Hodge 301. A sparsely populated red giant branch and red clump of the old field population can be seen in the Hodge 301 CMD at $0\overset{\mathrm{m}}{.}5 < (V-I)_0 < 1\overset{\mathrm{m}}{.}2$ and $-2$ mag $< M_V <$ 1 mag.

Fig. 5.— Magnitude histogram for the PC data of Hodge 301 (solid line). The incompleteness derived from artificial star experiments is indicated by long dashed lines in the faintest magnitude bins. No attempt was made to correct the last bin, which is severely affected by incompleteness. The luminosity function of Hodge 301 is compared to a luminosity function (LF) derived by Hunter et al. (1995; adapted from the completeness-corrected upper solid line in their Figure 19) for R 136. The R 136 LF ends where Hunter et al. (1995) considered the incompleteness too large for reasonable corrections. The LF of Hodge 301 extends to fainter magnitudes due to significantly less crowding in this sparse cluster as compared to the R 136 0.7 – 1.4 kpc annulus. At $M_{V,0} \sim 0\overset{\mathrm{m}}{.}3$ pre-main-sequence stars begin to appear in R 136 (see Figure 4). Hunter et al.'s (1995) LF was normalized to coincide with $M_{V,0} = -2$ to $-3$ magnitude bin of Hodge 301 (arbitrarily chosen). The brightest magnitude bins of Hodge 301 are affected by small-number statistics and the lack of stars near the main-sequence turnoff.

Fig. 6.— A two-color diagram to identify stars with H$\alpha$ excess. The H$\alpha$ magnitudes are instrumental. The bulk of main-sequence stars (MS) and supergiants (SGs) shows a scattered distribution around $(V - H\alpha) \sim 0$. We consider blue stars with $(V - H\alpha) > 0\overset{\mathrm{m}}{.}4$ to be Be star candidates.

Fig. 7.— Histogram of the number of Be star candidates (filled areas) and B main-sequence stars without emission (white areas) as a function of photometrically estimated spectral type. Numbers in the top row indicate the number ratio Be/(Be+B). The highest frequency of B emission star candidates is found among the early spectral types.

Fig. 8.— The slope of Hodge 301's mass function is $-1.38$ with a formal error of $\pm 0.07$, which is consistent with a Salpeter slope. The highest and the lowest mass bins (open circles) were excluded from the calculation of the slope to minimize incompleteness and evolutionary effects.

Fig. 9.— Distribution of stellar generations of differing age in 30 Dor. The location of our *WFPC2* field is indicated. Spectral classifications were taken from Walborn & Blades (1997), Parker (1993), and references therein. Upper left panel: The oldest generation as traced by K, M and A supergiants corresponding to ages of $\approx$ 20 Myr. The dot-dashed lines mark the approximate location of regions filled

with diffuse X-ray emission (after Wang 1999). Upper right panel: Distribution of B ($\approx>$ 10 Myr) and O ($\approx>$ 3 Myr) supergiants. The dashed circle encloses the R 143 association, which contains mainly late O and early B supergiants (Walborn & Blades 1997). R 143 itself is the only known luminous blue variable in the 30 Dor region (Parker et al. 1993) and believed to be younger than 7 Myr (Walborn & Blades 1997). Lower left panel: Location of early O main-sequence stars and Wolf-Rayet stars (ages $\approx<$ 5 Myr). Note that many of the W-R stars are believed to be very young main-sequence stars with ages of only 1 – 2 Myr. R 136 (dashed circle) contains a large number of such W-R stars and O3 stars (Massey & Hunter 1998), which are not marked individually. Lower right panel: Some of the locations of embedded protostars and star-forming regions along dense filaments (Walborn et al. 1999; Grebel et al., in prep.).

TABLE 1

LOG OF THE *HST* WFPC2 OBSERVATIONS OBTAINED ON 1995 DECEMBER 17.

| Filter | Exposure time [sec] | Gain [$e^-$/ADU] | CTE correction (PC1) [%] | Image root name |
|---|---|---|---|---|
| F656N | $2 \times 700$ | 7 | 2 | u3010101t, u3010102t |
| F555W | 4 | 15 | 4 | u3010103t |
| F555W | 40 | 7 | 4 | u3010104t |
| F555W | $2 \times 200$ | 7 | 4 | u3010105t, u3010106t |
| F336W | 10 | 15 | 4 | u3010109t |
| F336W | $2 \times 100$ | 7 | 4 | u301010at, u301010bt |
| F814W | 5 | 15 | 4 | u301010et |
| F814W | $2 \times 100$ | 7 | 4 | u301010ft, u301010gt |

TABLE 2

CROSS IDENTIFICATIONS, SPECTRAL TYPES, AND REDDENING OF PREVIOUSLY STUDIED STARS IN HODGE 301.

| MG73 (1) | MH81 (2) | Mk85 (3) | HSJG92 (4) | H93[a] (5) | WB97 (6) | SpT (7) | UIT SpT (8) | $A_V$ MH81 (9) | $E_{B-V,F}$ (10) | $E_{B-V,FS}$ (11) |
|---|---|---|---|---|---|---|---|---|---|---|
| MG 91 | Dor IR 4 | R 132[b] | HSJG 4 | UIT 269 | WB 1 | B0.5 Ia[d] | B3-5 I | | 0.14 | 0.00 |
| | | B2 | HSJG 6 | | WB 3 | A Ib[d] | | | | |
| MG 93 | Dor IR 35 | | HSJG 9 | | WB 4 | M I[c] | | 1.00 | | |
| MG 94 | Dor IR 7 | | HSJG 10 | | WB 5 | M I[c] | | 0.93 | | |
| | | | HSJG 7 | UIT 264 | WB 6 | B2 III[e] | O7-B0 V | | 0.09 | 0.16 |
| MG 95 | Dor IR 8 | | HSJG 11 | | WB 7 | M I[c] | | 0.96 | | |
| | | | | UIT 275 | WB 8 | B5: p[e] | O9-B0 VI | | 0.15 | 0.24 |
| | | | | UIT 250 | WB 9 | B2 V var[e] | O5-6 III | | 0.11 | 0.38 |
| | | B1 | HSJG 13 | | WB 10 | A0 Ib[d] | | | | |
| | | B3 | HSJG 16 | UIT 265 | WB 11 | A5 Ib[d] | B1-1.5 V | | 0.09 | 0.09 |
| | | | | UIT 241 | | | O3-6 V | | 0.09 | 0.49 |
| | | | | UIT 247 | | | B3-5 I | | 0.16 | 0.02 |
| | | | | UIT 256 | | | B3-5 I | | 0.09 | 0.06 |
| | | | | UIT 257 | | | | | 0.16 | 0.01 |
| | | | | UIT 258 | | | O7-B0 V | | 0.09 | 0.15 |
| | | | | UIT 259 | | | O7-B0 V | | 0.09 | 0.14 |

[a] Due to the large difference in resolution it is difficult to unambiguously identify the *UIT* stars in our *HST* image. The cross identifications listed here represent our best guess.

[b] Nomenclature from Feast et al. (1960).

[c] Spectral type from McGregor & Hyland (1981; MH81).

[d] Spectral type from Melnick (1985; Mk85).)

[e] Spectral type from Walborn & Blades (1997; WB97).

TABLE 3

COORDINATES AND PHOTOMETRY FOR BE STARS AND OTHER BRIGHT STARS IN HODGE 301.

| H93[a] (1) | WB97 (2) | $\alpha$ (J2000)[b] (3) | $\delta$ (J2000)[b] (4) | Be star (5) | $m_{162}$ (6) | $m_{189}$ (7) | $m_{221}$ (8) | $m_{256}$ (9) | $U_0$ (10) | $B$ (11) | $V_0$ (12) | $I_0$ (13) | $K$ (14) |
|---|---|---|---|---|---|---|---|---|---|---|---|---|---|
| UIT 269 | WB 1 | $5^h38^m15^s$ | $-69°03'47''$ | | 12.26 | 12.46 | 12.24 | 12.41 | | 13.05 | | 12.26[c] | |
| UIT 256 | WB 2 | $5^h38^m15.1^s$ | $-69°04'00''$ | no | 11.96 | 12.31 | 12.26 | 12.77 | 12.70 | 13.11 | 13.66 | 13.90 | |
| | WB 3 | $5^h38^m15.4^s$ | $-69°04'02''$ | no | | | | | 12.82 | | 12.12 | 11.94 | |
| | WB 4 | $5^h38^m16.7^s$ | $-69°04'13''$ | no | | | | | 16.17 | | 13.40 | 11.16 | 8.39 |
| | WB 5 | $5^h38^m17.0^s$ | $-69°04'00''$ | no | | | | | 15.83 | | 13.00 | 11.16 | 8.70 |
| UIT 264 | WB 6 | $5^h38^m17.0^s$ | $-69°03'49''$ | Be4 | 12.53 | 13.09 | | 13.43 | 14.15 | 15.45 | 15.34 | 15.56 | |
| | WB 7 | $5^h38^m17.6^s$ | $-69°04'11''$ | no | | | | | 16.15 | | 13.29 | 11.76 | 8.87 |
| UIT 275 | WB 8 | $5^h38^m18.0^s$ | $-69°03'38''$ | | 13.61 | 13.69 | | 14.39 | | 15.11 | | | |
| UIT 250 | WB 9 | $5^h38^m18.0^s$ | $-69°04'08''$ | Be1 | 12.78 | 13.05 | | 13.41 | 12.83 | 14.64 | 13.80 | 13.75 | |
| | WB 10 | $5^h38^m18.3^s$ | $-69°04'01''$ | no | | | | | 12.71 | | 12.49 | 12.45 | |
| UIT 265 | WB 11 | $5^h38^m22.0^s$ | $-69°03'47''$ | | 13.71 | | | 15.01 | | 16.92 | | | |
| UIT 257 | | $5^h38^m18.8^s$ | $-69°03'59''$ | Be3 | 12.44 | 12.87 | 11.91 | 13.00 | 14.22 | 13.36 | 15.27 | 15.24 | |
| UIT 259 | | $5^h38^m16.0^s$ | $-69°03'53''$ | Be2 | 12.42 | 12.68 | | 13.58 | 13.90 | 15.50 | 15.15 | 15.21 | |
| UIT 247 | | $5^h38^m19.7^s$ | $-69°04'09''$ | no | | 14.31 | | 14.73 | 14.34 | 16.25 | 15.50 | 15.66 | |
| UIT 241 | | $5^h38^m16.5^s$ | $-69°04'13''$ | no | 13.66 | | | 14.62 | 14.90 | 15.53 | 16.06 | 16.32 | |
| UIT 258 | | $5^h38^m17.0^s$ | $-69°04'01''$ | no | 12.61 | 13.04 | | 13.33 | 14.36 | 15.23 | 15.53 | 15.77 | |
| | | $5^h38^m15.6^s$ | $-69°04'01''$ | Be5 | | | | | 14.18 | | 15.35 | 15.29 | |
| | | $5^h38^m18.7^s$ | $-69°03'58''$ | Be6 | | | | | 14.31 | | 15.48 | 15.65 | |
| | | $5^h38^m16.8^s$ | $-69°03'56''$ | Be7 | | | | | 14.88 | | 15.70 | 15.78 | |
| | | $5^h38^m16.4^s$ | $-69°03'50''$ | Be8 | | | | | 14.86 | | 16.01 | 15.98 | |
| | | $5^h38^m17.3^s$ | $-69°03'55''$ | Be9 | | | | | | | 16.25 | 16.19 | |
| | | $5^h38^m17.0^s$ | $-69°03'50''$ | Be10 | | | | | | | 16.32 | 16.31 | |
| | | $5^h38^m17.3^s$ | $-69°04'01''$ | Be11 | | | | | | | 16.45 | 16.57 | |
| | | $5^h38^m16.8^s$ | $-69°03'54''$ | Be12 | | | | | 15.59 | | 16.68 | 16.83 | |
| | | $5^h38^m15.7^s$ | $-69°03'53''$ | Be13 | | | | | 15.63 | | 16.73 | 16.67 | |
| | | $5^h38^m18.7^s$ | $-69°04'03''$ | Be14 | | | | | 16.74 | | 17.20 | 17.24 | |
| | | $5^h38^m15.7^s$ | $-69°03'47''$ | Be15 | | | | | 16.37 | | 17.36 | 17.46 | |
| | | $5^h38^m17.6^s$ | $-69°03'56''$ | Be16 | | | | | 16.61 | | 17.53 | 17.64 | |
| | | $5^h38^m15.5^s$ | $-69°03'56''$ | Be17 | | | | | 16.86 | | 17.69 | 17.76 | |
| | | $5^h38^m15.9^s$ | $-69°03'59''$ | Be18 | | | | | 17.23 | | 18.10 | 18.26 | |
| | | $5^h38^m16.3^s$ | $-69°03'57''$ | Be19 | | | | | | | 18.66 | 18.88 | |

[a] Due to the large difference in resolution it is difficult to unambiguously identify the *UIT* stars in our *HST* image. The cross identifications listed here represent our best guess.

[b] The equatorial coordinates were determined with the task METRIC in STSDAS on the PC image. The coordinates for the stars WB1, WB8, and WB11 were determined on images from the Digitized Sky Survey using the IRAF/PROS task TVLABEL.

[c] Undereddened $I$ magnitude from Mendoza & Gómez (1973).

TABLE 4
MASS RANGE, MAGNITUDE BINS[1] AND MAIN-SEQUENCE STAR COUNTS FOR HODGE 301.

| Mass range ($M_\odot$) | log ($M/M_\odot$) | $M_V$ | $N$ |
|---|---|---|---|
| 10.0 – 7.9 | 1.0 | -2.90 | $21 \pm 4.6$ |
| 7.9 – 6.3 | 0.9 | -1.83 | $21 \pm 4.6$ |
| 6.3 – 5.0 | 0.8 | -1.11 | $44 \pm 6.6$ |
| 5.0 – 4.0 | 0.7 | -0.51 | $60 \pm 7.7$ |
| 4.0 – 3.2 | 0.6 | 0.07 | $57 \pm 7.5$ |
| 3.2 – 2.5 | 0.5 | 0.65 | $71 \pm 8.4$ |
| 2.5 – 2.0 | 0.4 | 1.24 | $119 \pm 10.9$ |
| 2.0 – 1.6 | 0.3 | 1.90 | $183 \pm 13.5$ |
| 1.6 – 1.3 | 0.2 | 2.64 | $243 \pm 15.6$ |
| 1.3 – 1.0 | 0.1 | 3.74 | $305 \pm 17.5$ |

[1]Logarithmic mass and magnitude entries denote the upper boundaries of each mass and magnitude bin.


This figure "grebel.fig1.jpg" is available in "jpg" format from:
http://arXiv.org/ps/astro-ph/9910426v1


This figure "grebel.fig2.jpg" is available in "jpg" format from:
http://arXiv.org/ps/astro-ph/9910426v1

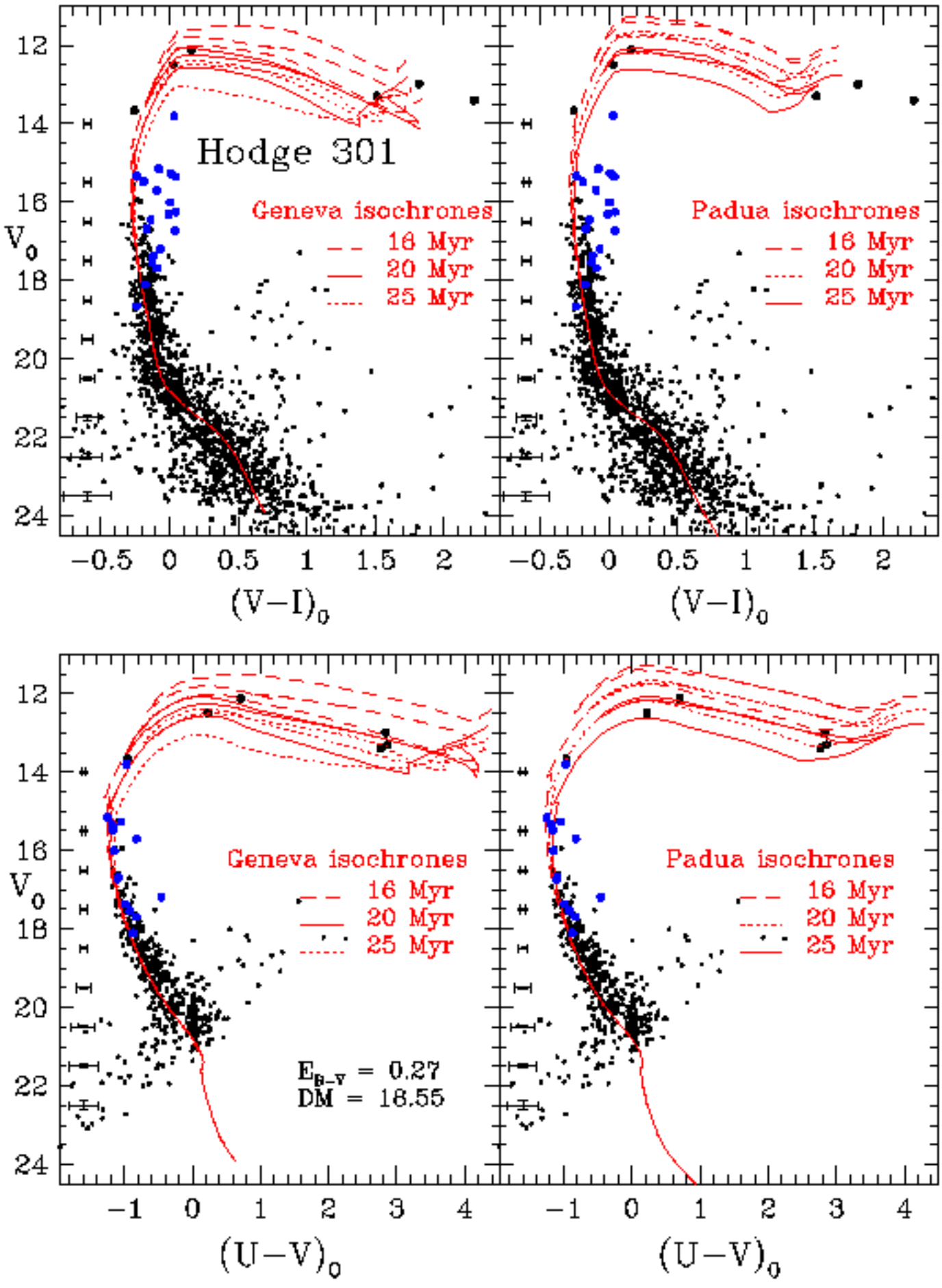
Hodge 301
Geneva isochrones
16 Myr
20 Myr
25 Myr
Padua isochrones
16 Myr
20 Myr
25 Myr
$V_0$
$(V-I)_0$
$(U-V)_0$
$E_{B-V}$ = 0.27
DM = 18.55

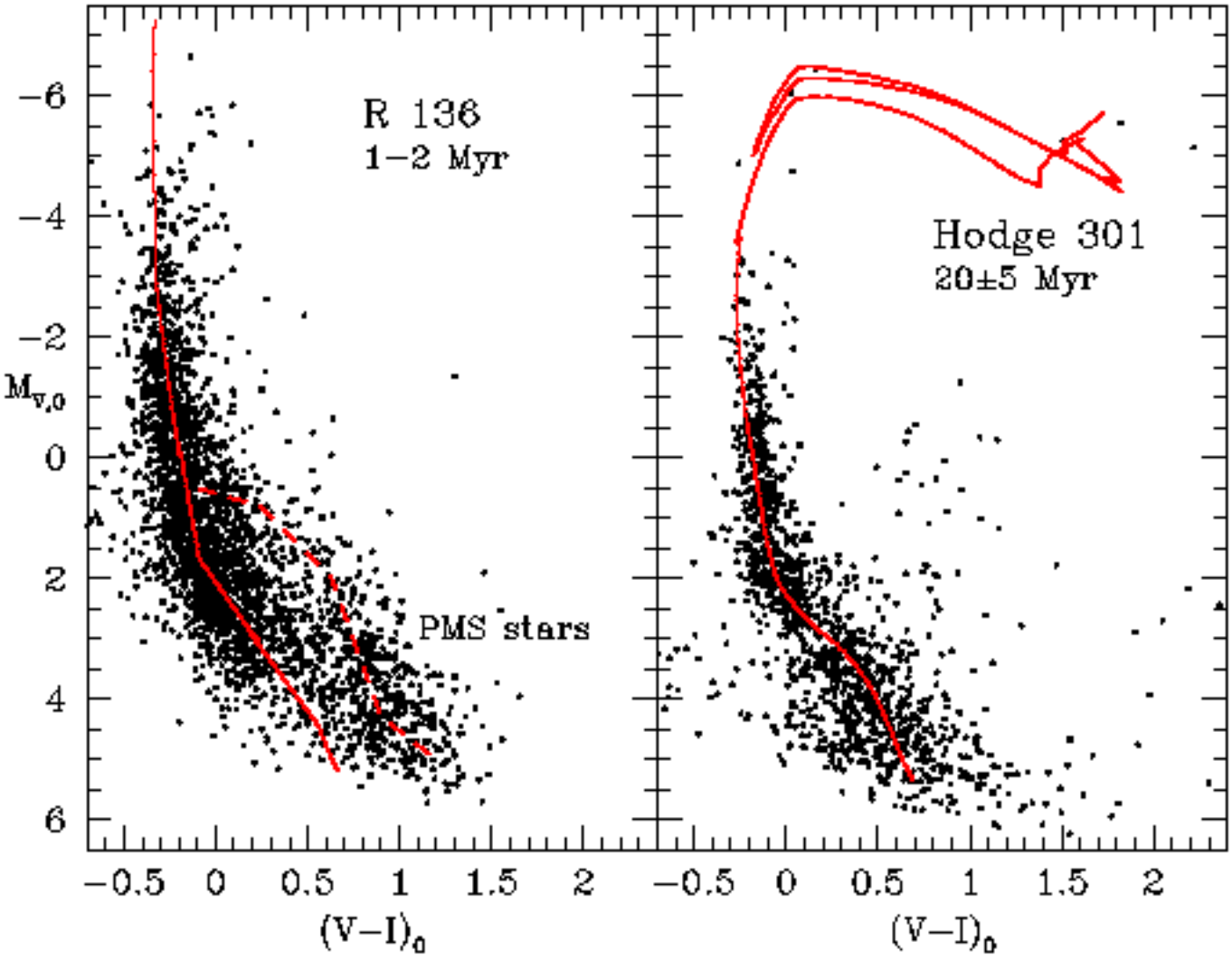
R 136
1–2 Myr
PMS stars
Hodge 301
20±5 Myr
$M_{V,0}$
$(V-I)_0$
$(V-I)_0$
−6
−4
−2
0
2
4
6
−0.5
0
0.5
1
1.5
2

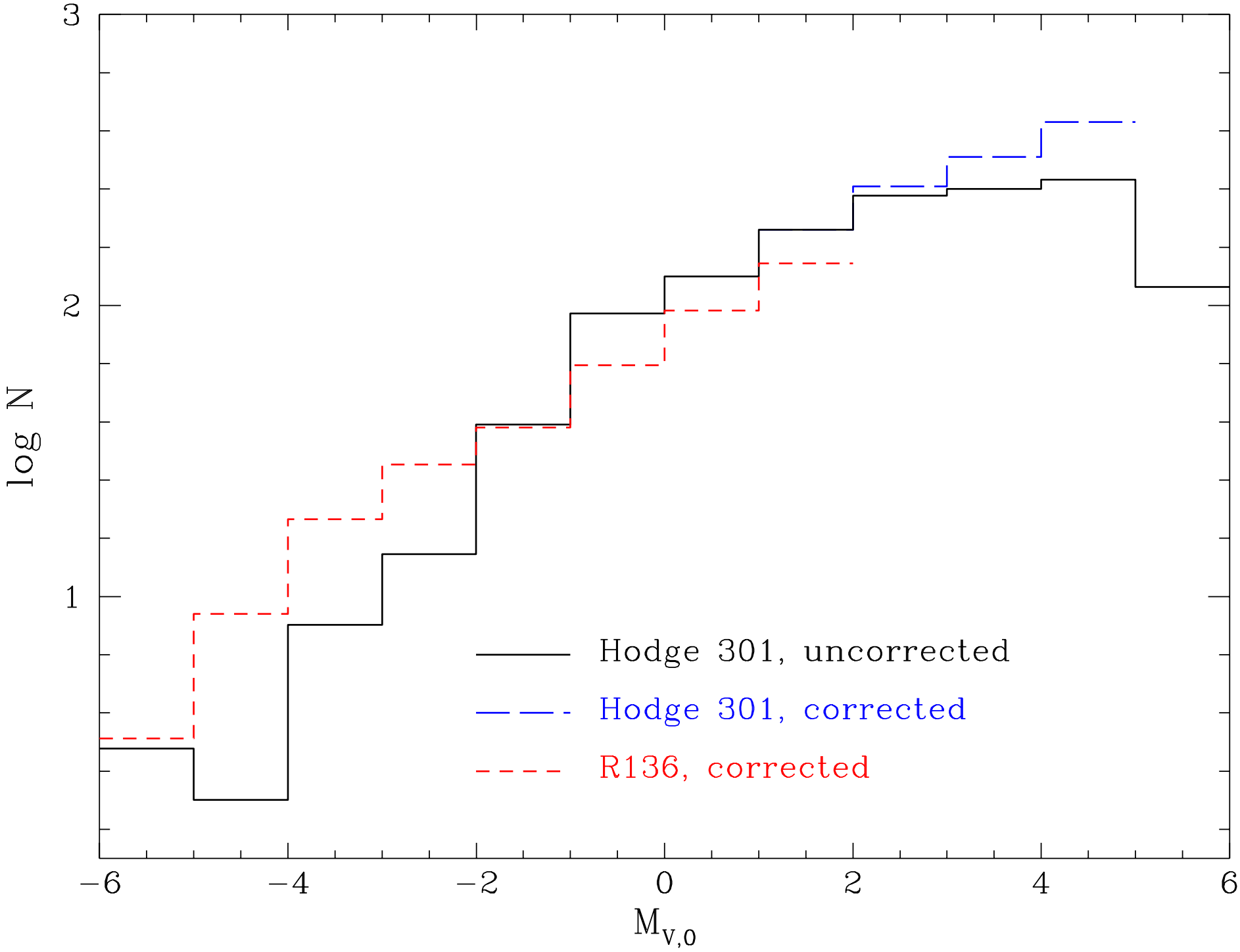
3
2
1
log N
−6
−4
−2
0
2
4
6
$M_{V,0}$
Hodge 301, uncorrected
Hodge 301, corrected
R136, corrected

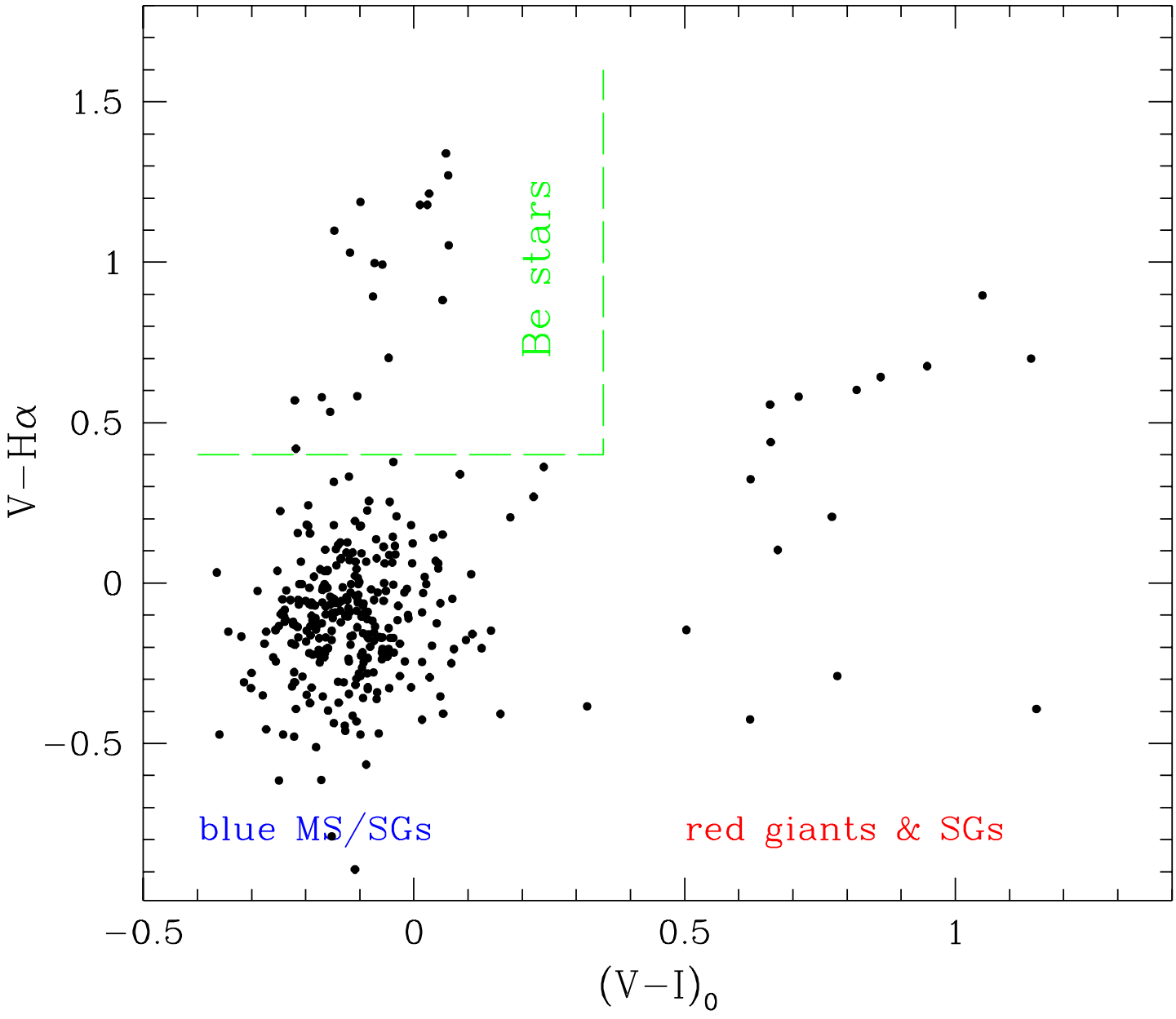
1.5
1
0.5
0
−0.5
V−Hα
Be stars
blue MS/SGs
red giants & SGs
−0.5
0
0.5
1
(V−I)0

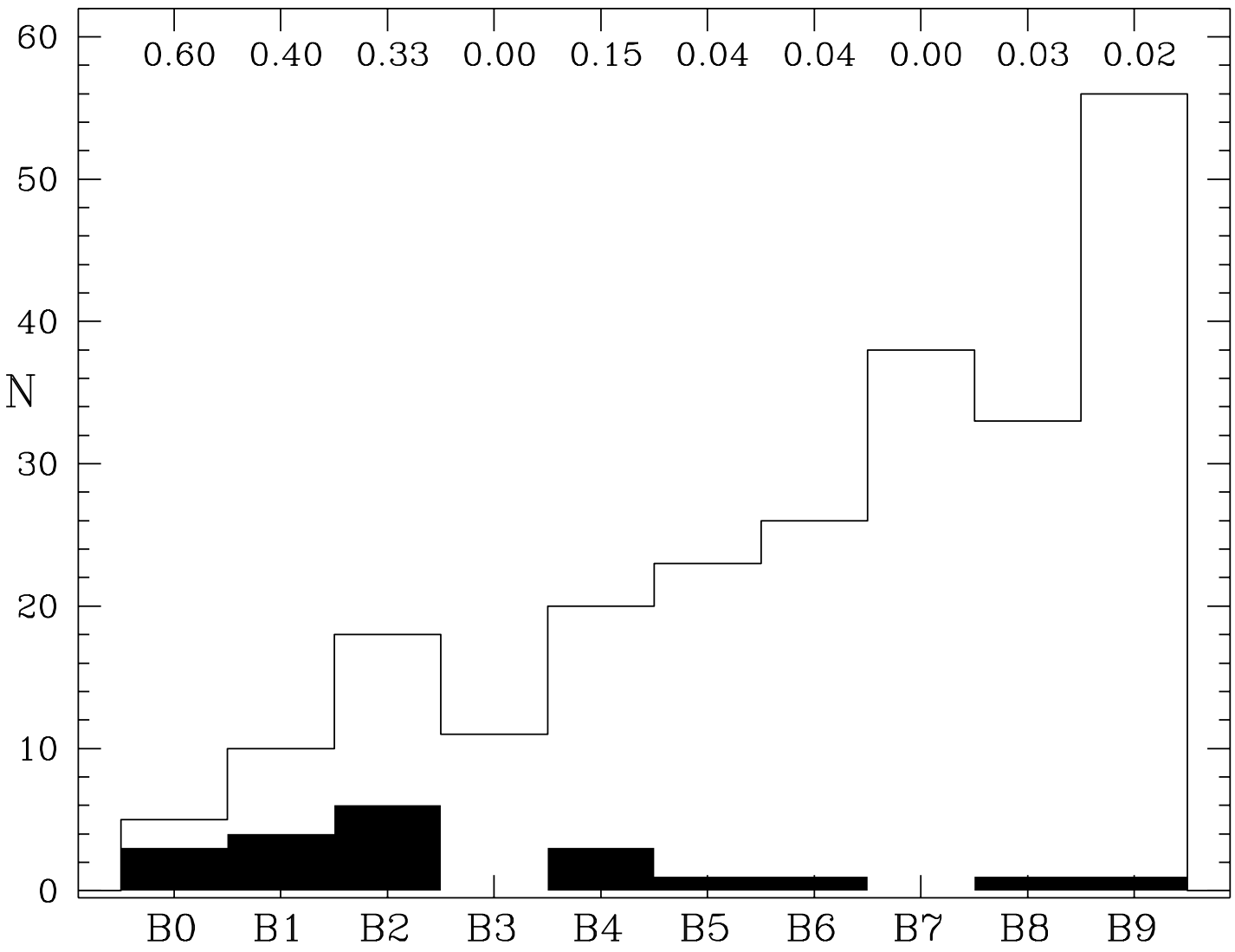
0.60 0.40 0.33 0.00 0.15 0.04 0.04 0.00 0.03 0.02
60
50
40
N
30
20
10
0
B0 B1 B2 B3 B4 B5 B6 B7 B8 B9

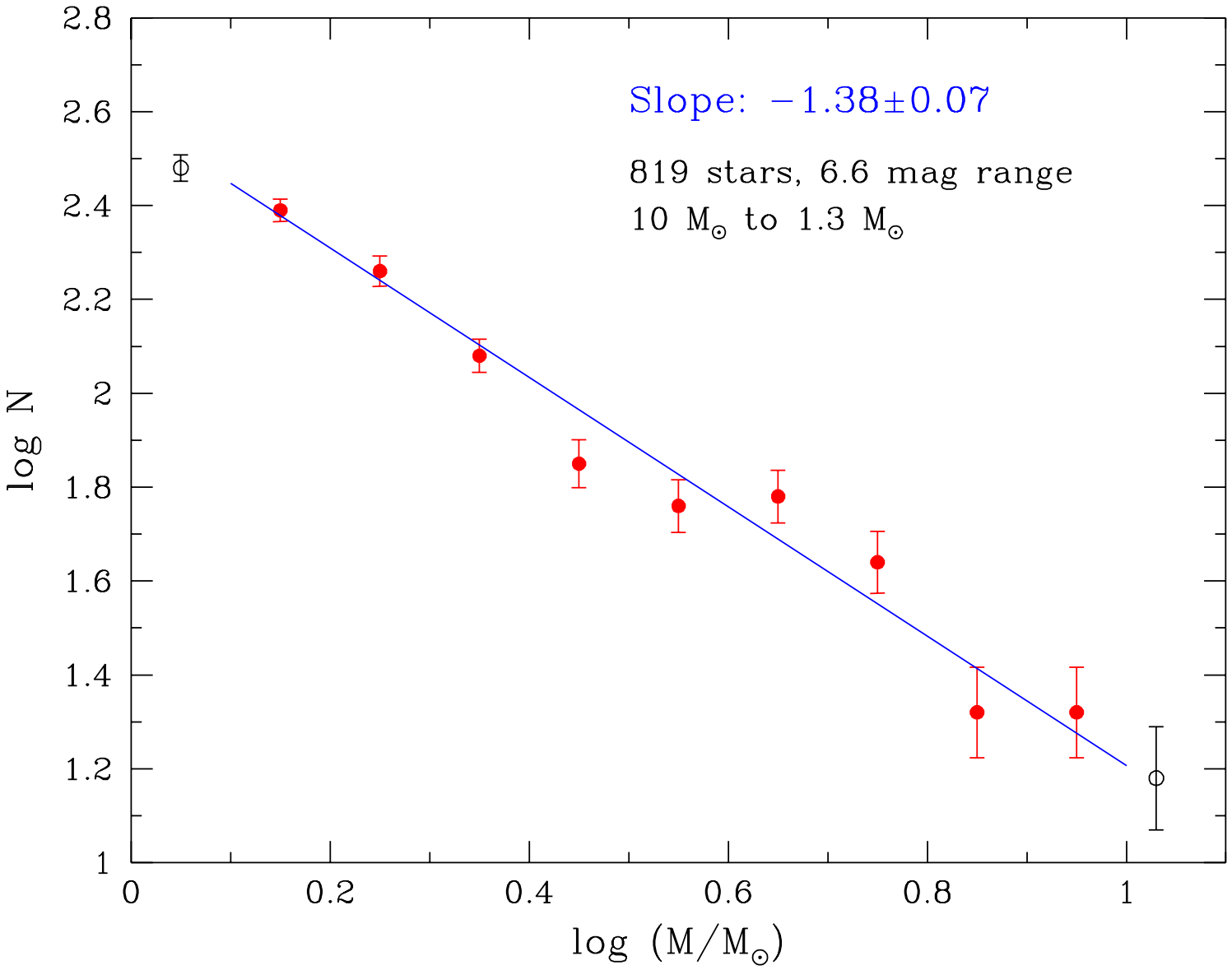
Slope: −1.38±0.07
819 stars, 6.6 mag range
10 M⊙ to 1.3 M⊙
log N
log (M/M⊙)
2.8
2.6
2.4
2.2
2
1.8
1.6
1.4
1.2
1
0
0.2
0.4
0.6
0.8
1


This figure "grebel.fig9.jpg" is available in "jpg" format from:
http://arXiv.org/ps/astro-ph/9910426v1